2024 IEEE/RSJ International Conference on Intelligent Robots and Systems (IROS)
October 14-18, 2024. Abu Dhabi, UAE

Improved Contact Stability for Admittance Control of Industrial Robots with Inverse Model Compensation

Kangwagye Samuel, Kevin Haninger, Sami Haddadin, and Sehoon Oh

***Abstract*— Industrial robots have increased payload, repeatability, and reach compared to collaborative robots, however, they have a fixed position controller and low intrinsic admittance. This makes realizing safe contact challenging due to large contact force overshoots in contact transitions and contact instability when the environment and robot dynamics are coupled. To improve safe contact on industrial robots, we propose an admittance controller with inverse model compensation, designed and implemented outside the position controller. By including both the inner loop and outer loop dynamics in its design, the proposed method achieves expanded admittance in terms of increasing both gain and cutoff frequency of the desired admittance. Results from theoretical analyses and experiments on a commercial industrial robot show that the proposed method improves rendering of the desired admittance while maintaining contact stability. We further validate this by conducting actual assembly tasks of plug insertion with fine positioning, switch insertion onto the rail, and colliding the robot end effector with random objects and surfaces, as seen at `https://youtu.be/8XfkdHEdWDs`.**

I. Introduction

Efforts to extend the utilization of industrial robots in complex contact-rich collaborative tasks have recently increased [1], [2]. Such tasks include a wide range of applications, from precision assembly tasks like inserting gears, switches, and pins [3], [4], to everyday actions such as opening doors by grasping handles [5]–[7]. The complexity of these tasks, characterized by the coupling of the robot with its environment, poses a big challenge to ensuring smooth contact transitions [8]. Thus, smooth interaction between the robot manipulator and the dynamic environments is essential for accomplishing such contact-rich tasks. This can be resolved by implementing admittance control on the robots.

In complex contact-rich co-manipulation assembly tasks, one fundamental challenge is achieving an expanded admittance while maintaining contact stability. In this paper, *expanded admittance* refers to ability to increase both the admittance gain and the frequency within which the desired admittance can be rendered leading to increased manipulation speed while ensuring contact stability. While advanced admittance control methods developed for collaborative robots have proven to be effective in achieving expanded admittance and contact stability [9]–[11], the case of typical industrial robots still exhibit challenges. This is because commercial industrial robots are equipped with "black box" position controller that can not accessed for design tuning. Moreover, these robotic systems have low admittance due to their heavy structure which leads to large contact forces [12], [13]. In addition, modeling the intricacies of these environments the robot interacts with remains a big challenge.

A basic task space admittance controller utilizes end-effector Force/Torque (F/T) sensor measurements, sending commands to an inner-loop position control [9], [14]. With this technique, the inner position controller is maintained, moreover, environment modeling is also not required. However, the basic admittance control approach exhibits a fundamental limitation – increasing admittance often comes at the cost of deteriorating contact stability [15]. Techniques such as a lead filter [16], an inverse feedforward filter [17], or a finite-impulse response filter [18] can reduce collision forces. Model-based methods can use the robot dynamic and measured inputs/outputs to improve the control. A conventional disturbance observer (DOB) [19] has been shown to improve force [20] and admittance control [21]. However, this method emphasizes stiff position control by suppressing the effects of disturbances, increasing impact forces. A Dist-Add method was introduced in [22] as a strategy towards enhancing inner-loop admittance without compromising contact stability. Using positive velocity feedback and disturbance addition, the admittance was increased. However, this approach primarily focuses on increasing inner-loop admittance.

In this paper, we propose extending a standard DOB in [21] with a compensator on measured force to expand the admittance which is safe in contact. The proposed method uses a model of inner-loop robot dynamics in the outer-loop admittance control to cancel inner-loop dynamics and thus more accurately render a desired admittance. Moreover, by utilizing the F/T sensor measurements, our approach indirectly takes into account the dynamics of contact, actively suppressing their effects. The proposed approach is validated on an industrial robot in contact transition with a range of environments, and shown to improve contact stability and reduce force overshoot. The proposed method contributes to the efforts towards extending the applications of commercial

This work was supported in part by the Technology Innovation Program (20015101) funded by the Ministry of Trade, Industry & Energy (MOTIE, Korea), in part by the DGIST R&D Program of the Ministry of Science and ICT (23-PCOE-02), in part by the European Union's Horizon 2020 research and innovation programme under grant agreement No 101058521 — CONVERGING, and in part by the Lighthouse Initiative Geriatronics by StMWi Bayern Project X under Grant IUK-1807-0007// IUK582/001.

Kangwagye Samuel and Sami Haddadin are with the Chair of Robotics and Systems Intelligence, Munich Institute of Robotics and Machine Intelligence (MIRMI), Technical University Munich, 80992 Munich, Germany. Kangwagye Samuel is also with the Department of Mechanical and Production Engineering, Kyambogo University, Kampala, Uganda (`s.kangwagye@tum.de; haddadin@tum.de`).

Kevin Haninger is with the Department of Automation, Fraunhofer IPK, 10589 Berlin, Germany (`kevin.haninger@ipk.fraunhofer.de`).

Sehoon Oh is with the Department of Robotics and Mechatronics Engineering, DGIST, Daegu 42988, Korea (`sehoon@dgist.ac.kr`).

industrial robots from conventional caged practices to sharing the same workspace with human co-workers.

This paper is organized as follows. Section II discusses the complex contact-rich assembly tasks problem while Section III presents the design and analysis of the proposed method. Experiments are conducted in Section IV and the conclusion is given in Section V.

II. Description of the Contact-Rich Co-Manipulation Assembly Tasks

This section introduces the industrial robot utilization in contact-rich tasks and its admittance control using basic and DOB-based techniques. Moreover, the challenges of admittance and contact stability for these methods are discussed.

A. Industrial Robot Utilization in Contact-Rich Tasks

Fig. 1(a) illustrates a typical commercial industrial robot. This is a 6-DOF COMAU Racer-7-1.4 robot equipped with a "black box" position/velocity/current controller. To measure the end effector forces, a 6-DOF force/torque (F/T) sensor is coupled to its flange, and then the gripper rigidly fixed to the F/T sensor. On the right of Fig. 1(a) are two examples of assembly tasks with environmental contacts: the top one is a switch insertion co-manipulation task which involves multiple contacts, and in the bottom figure, an autonomously operated robot is making contact with a stiff surface. Execution of these tasks is realized by admittance control where the F/T sensor measurements are utilized in the outer loop, as discussed in Section III.

1) Task Execution with Co-manipulation (Manual Guidance) of the Robot: The step-wise execution of the switch insertion task in Fig. 1(a) right-top is shown in details in Fig. 1(b). It shows the transitions from free space motion to contact with coupling between the environment and the robot, and this action is executed by human applying force, F_{hum}, to guide the admittance-controlled robot. This operation can be explained in two stages, i.e., in stage 1 when the robot is being guided in free space before and after contact, this is admittance control stage. And stage 2 when the robot is contacting a stiff surface during task execution, this is a combination of both pure force control and admittance control due to very small motions.

2) Task Execution with the Robot Under Autonomous Operation: Fig. 1(c) presents the detail of an autonomously operated robot whose end-effector is making contact with a high-stiffness surface. The autonomous mode is executed by supplying the desired virtual force trajectory, F_r, where the robot is made to move and make contact with the surface with vertical motions only. Three scenarios are presented, i.e., (i) contact on soft surface, (ii) contact on hard surface, and (iii) contact on soft surface with extra load added to the end-effector. As with manual guidance, each of the autonomous operation in Fig. 1(c) also consists of free space motion stage with admittance control and the contact stage with pure force control.

The assembly tasks illustrated in Fig. 1 pose a big challenge, e.g., switch insertion in (b) involves continuous

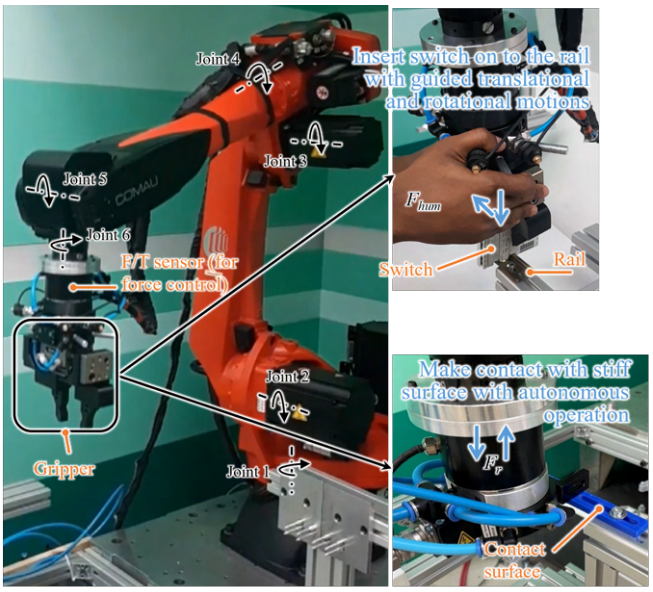

(a) The robot (left) with tasks for manual (right-top) guidance and autonomous (right-bottom) operation.

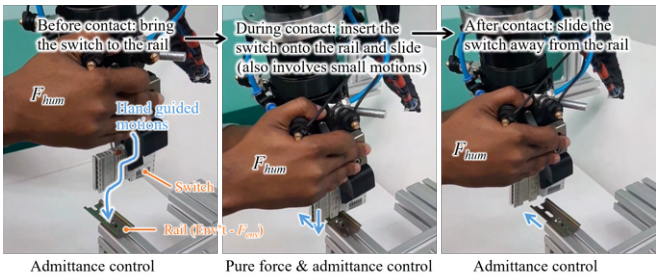

(b) Detailed demonstration of the step-wise execution of the contact-rich co-manipulation task. Free space motion - contact transition description using a task of inserting a switch on to a rail.

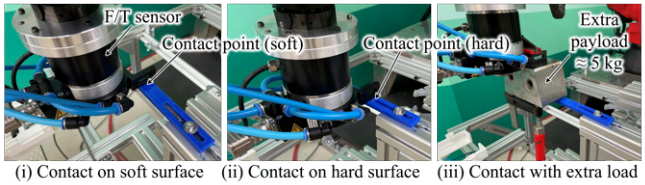

(c) Three cases of contact control with autonomous robot operation.

Fig. 1. Illustration of a typical commercial industrial robot utilization in contact-rich assembly tasks under admittance control in task space.

coupling between the switch and the rail with multiple contacts whereas the task in (c) involves colliding with a high stiffness surface which generates large contact forces. Executing these tasks safely require higher admittance and wide bandwidth.

B. Basic and DOB-Based Admittance Control Methods

The block diagram in Fig. 2 presents the basic (green color) [16] and DOB-based (blue color) [21], [22] admittance control methods for a single DOF in task space.

As illustrated in Fig. 2, the robot in Fig. 1 can either be manipulated manually by human through F_{hum} [as in

Fig. 1(b)] or operated autonomously through the virtual reference force F_r [as in Fig. 1(c)]. The F/T sensor measures the interaction force, F, physically acting on the robot dynamics, $R(s)$, and the measured force, F_m, is used for outer-loop feedback. An inner-loop task space motion controller, $C(s)$, tracks the motion command, V_i, supplied by the admittance controller, $A(s)$. In addition, $P(s)$ and $E(s)$ are payload (gripper) and environment (high-stiffness contact surface), respectively. These dynamics are given in Laplace domain considered for a single DOF as

$$R = \frac{1}{M_r s + B_r},\ C = k_p + \frac{k_i}{s},\ P = \frac{1}{M_p s},$$
$$T = \frac{CR}{1+CR},\ A = \frac{1}{M_a s + B_a},\ E = \frac{K_e}{s}, \tag{1}$$

where M_r and B_r are robot mass and damping, k_p and k_i are proportional and integral coefficients, M_p is payload mass, M_a and B_a are desired admittance mass and damping coefficient, and K_e is environment stiffness. The Laplace operator s is ignored on the transfer functions in (1), and from herein after for simplicity.

Admittance control of Fig. 1 is realized about a compliant frame (typically the robot's Tool Center Point (TCP)), where the total control is diagonal and each DOF is independent. The force measurements are transformed into this frame before payload compensation, and the robot motion is commanded in this frame. In addition, the admittance control model in Fig. 2 is in task space and assumed to be linearized and diagonal (i.e., each task space DOF is independent) [16], [22], thus, a single DOF is analyzed in this paper as shown in (1). A linear model allows the use of frequency-domain analysis of contact resonance and rendered admittance.

Both of these approaches do not require knowledge of the environment model. The basic method (green color) [16], [22] only utilizes the F/T sensor measurements as feedback. On the other hand, the DOB-based method (green color) [21], abbreviated as dob from herein after, is based on estimating external disturbances to the robot motion by using the measured output, an inverse model, and the measured input [19]. T_n is the nominal model of the inner-loop robot dynamics, T, and Q is the Q-filter designed as a first-order LPF to make T_n proper as shown below

$$T_n = \frac{C_n R_n}{1 + C_n R_n} \ \text{ and } \ Q = \frac{\omega^Q}{s + \omega^Q}, \tag{2}$$

where ω^Q is the Q-filter cutoff frequency.

With the dob method, the estimated disturbances are compensated at the command input to ensure stiff position control. Typical disturbances for industrial manipulators are high friction, mechanical vibrations due to higher-order dynamics, and coupling between degrees of freedom in task space due to imperfections in joint-level control. Here, we also consider that the external forces act on the robot system, causing deviation from the expected motion control performance.

The basic and dob methods exhibit limitations when executing complex contact-rich assembly tasks as discussed next.

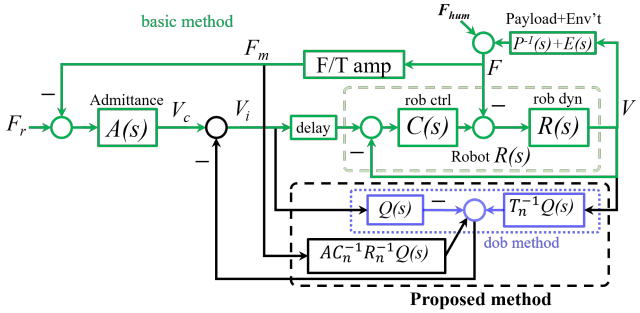

Fig. 2. Block diagram showing admittance control with: basic method in green color (or when $Q = 0$), dob method in blue color, and the proposed method in black color, which has an additional block to the dob method.

C. Admittance and Contact Stability Limitations of basic and dob Control Methods

It is desired that the inner-loop robot dynamics $T(s)$ equal to unity to track the set admittance, $A(s)$. In addition, the desired admittance should be increased while enhancing contact stability. These two objectives can be checked for the two methods by utilizing the transfer function for the rendered admittance $Y = -\mathcal{V}/\mathcal{F}_{hum} = -\mathcal{V}/\mathcal{F}$. This is given for the basic and dob methods, respectively, as shown below

$$Y^{\text{basic}} = T(A + C^{-1}), \tag{3}$$
$$Y^{\text{dob}} = \frac{T[A + C^{-1}(1-Q)]}{1 - Q + QT_n^{-1}T}. \tag{4}$$

It can be observed from (3) that rendering the desired admittance for the basic method is hindered by the dynamics of velocity-controlled robot and the physical impact of forces on the robot. Moreover, it was shown in [22] that increasing the admittance gain deteriorates the contact stability by reducing the phase of Y^{basic}.

For the case of the dob method in (4), $Y^{\text{dob}} = AT_n$ when $Q = 1$. Thus, the effect of the inner loop dynamics is eliminated, however, the desired admittance can only be rendered in the low frequency ranges when $|T_n| = 1$. This implies that the bandwidth of T_n limits the range within which the desired admittance can be rendered.

From the above, both methods exhibit the limitation of not expanding the admittance in both magnitude and frequency due to inner-loop dynamics and the impact of force on the robot dynamics.

III. Proposed Method

To overcome the limitations of basic and dob methods, the characteristics of both inner loop and outer loop dynamics are exploited to design the proposed method as shown in Fig. 2. Here, a block consisting of the admittance controller and inverse of the open loop velocity control dynamics is added to the dob method. This utilizes the F/T sensor measurements as the input to estimate high frequency contact dynamics which amplify contact forces, thus enhancing contact stability.

In the $AC_n^{-1}R_n^{-1}Q(s)$ block, $A(s)$ converts force into velocity as well as introducing the admittance behaviour,

$C_n^{-1}R_n^{-1}(s)$ estimates the disturbance velocity due to contact dynamics, and $Q(s)$ acts as a filter for noise attenuation. To this end, the output of $AC_n^{-1}R_n^{-1}Q(s)$ is high-frequency contact dynamics and this is added to the dob. Thus, the proposed method suppresses the effects of inner-loop disturbances and outer loop high-frequency contact forces.

A. Achieving Expanded Admittance with Contact Stability

The rendered admittance transfer function, $Y = -\mathcal{V}/\mathcal{F}_{hum} = -\mathcal{V}/\mathcal{F}$, representing both manual guidance and autonomous operations in Fig. 1(b)&(c) is derived for the proposed method and given below

$$Y^{\text{proposed}} = \frac{T[A + C^{-1}(1-Q) + AC_n^{-1}R_n^{-1}Q]}{1 - Q + QT_n^{-1}T}. \quad (5)$$

Compared to (4), the proposed method adds the outer loop characteristic, $AC_n^{-1}R_n^{-1}Q$, to the numerator of (5). When $Q = 1$, (5) becomes

$$Y_{Q=1}^{\text{proposed}} = AT_n(1 + C_n^{-1}R_n^{-1}) = AT_nT_n^{-1} = A. \quad (6)$$

Therefore, at higher Q-filter cutoff frequencies, the effect of inner-loop dynamics is eliminated and the desired admittance can be rendered without limitations. Further, if $A(s)$ in (6) is expressed as

$$A = \frac{1}{M_as + B_a} = \frac{1/B_a}{(M_a/B_a)s + 1} = \frac{k_a}{\tau_a s + 1}, \quad (7)$$

the admittance can be expanded by increasing the gain k_a and reducing the time constant τ_a. Thus, from (6) and (7), the expanded admittance objective is of increasing both the admittance gain and cutoff frequency is achieved.

Furthermore, the magnitude and phase characteristics of (3), (4), and (5) are plotted in Fig. 3 when the parameters are set as

$$R = \frac{1}{41.667s + 1000}, \quad C = 1425 + \frac{38000}{s}, \quad (8)$$

$$R_n = \frac{1}{16.667s + 400}, \quad C_n = 475 + \frac{19000}{s}, \quad (9)$$

and $\omega^Q = 15$ Hz. Two admittance controller settings of $A(s) = 1/(8s + 800)$ and $A(s) = 1/(4s + 400)$ are used to test the system behavior at low and high admittance gains.

The magnitude plots in Fig. 3(top) show that as compared to the basic and dob methods, the proposed method tracks the desired admittance better with increased cutoff frequency. Thus, with the proposed method, the overall admittance gain and bandwidth can be increased via the desired admittance setting without limitation.

The passivity approach is utilized here to evaluate the contact stability improvement by the proposed method [9], where a system is passive or contact stable if $\angle Y(s)$ lies between -90^o and 90^o, is often used as a contact stability condition in admittance control [9]. To this end, the phase characteristic shown in Fig. 3 shows that the proposed method improves the contact stability at both values of M_a and B_a, since the passivity condition is violated at higher frequencies, i.e., 22.26 Hz for 8,800 and 20.47 Hz for 4,400. On the other hand, the dob method shows good contact stability at low admittance gains (with passivity violation at 30 Hz) but exhibits poor contact stability at higher admittance gains (with passivity violation at 9.61 Hz). The basic method exhibits the same behavior as dob method where passivity condition is violated at 15.09 Hz and 12.08 Hz for small and large admittance gains, respectively.

B. Further Theoretical Evaluation of Reduced Peak Contact Forces and Enhanced Contact Stability

The contact forces at the robot-environment interface induced by the contact surface for manual guidance (co-manipulation) and autonomous operation can be represented by the transfer functions $G = \mathcal{F}/\mathcal{F}_{hum}$ and $H = \mathcal{F}/\mathcal{F}_r$, respectively. These are derived from Fig. 2 for all the three methods and given below.

$$G^{\text{basic}} = 1/\zeta_1, \quad (10)$$

$$H^{\text{basic}} = AT(P^{-1} + E)/\zeta_1, \quad (11)$$

$$G^{\text{proposed}} = (1 - Q + QT_n^{-1}T)/\zeta_2, \quad (12)$$

$$H^{\text{proposed}} = AT(P^{-1} + E)/\zeta_2, \quad (13)$$

$$G^{\text{dob}} = (1 - Q + QT_n^{-1}T)/\zeta_3, \quad (14)$$

$$H^{\text{dob}} = AT(P^{-1} + E)/\zeta_3, \quad (15)$$

where $\zeta_1 = 1 + T(A + C^{-1})(P^{-1} + E)$, $\zeta_2 = [1 + TC^{-1}(P^{-1}+E)](1-Q)+AT(P^{-1}+E)(1+QC_n^{-1}R_n^{-1})+QT_n^{-1}T$, and $\zeta_3 = [1+TC^{-1}(P^{-1}+E)](1-Q)+AT(P^{-1}+E) + QT_n^{-1}T$.

It can be observed for the basic method in (10) and (11) that the actual inner loop dynamics can amplify contact forces thus deteriorating contact stability. For dob and proposed methods, consider large values of ω^Q such that $Q = 1$, (12)-(15) become

$$G_{Q=1}^{\text{proposed}} = 1/[1 + A(P^{-1} + E)], \quad (16)$$

$$H_{Q=1}^{\text{proposed}} = AT_n(P^{-1} + E)/[1 + A(P^{-1} + E)], \quad (17)$$

$$G_{Q=1}^{\text{dob}} = 1/[1 + AT_n(P^{-1} + E)], \quad (18)$$

$$H_{Q=1}^{\text{dob}} = AT_n(P^{-1} + E)/[1 + AT_n(P^{-1} + E)]. \quad (19)$$

Thus, the actual inner loop dynamics are eliminated by the dob and proposed method. However, the nominal model is present in the denominators of the dob in (18) and (19), thus, limiting the control bandwidth which may affect contact stability especially at larger gains of admittance. This is absent for the proposed method in (16) and (17) showing that high frequency contact forces can be damped, enhancing contact stability since there is no bandwidth limitations.

To visualize the contact resonances, the magnitudes of (11), (17), and (19) are plotted in Fig. 4. The proposed method does not exhibit resonances in both soft ($K_e =$ 10kN/m) and hard ($K_e =$ 30kN/m) surfaces even at high admittance, i.e., when $M_a, B_a = 4, 400$. Moreover, addition of extra payload does not affect the proposed method. On the other hand, the basic and dob methods exhibit resonances in all the cases.

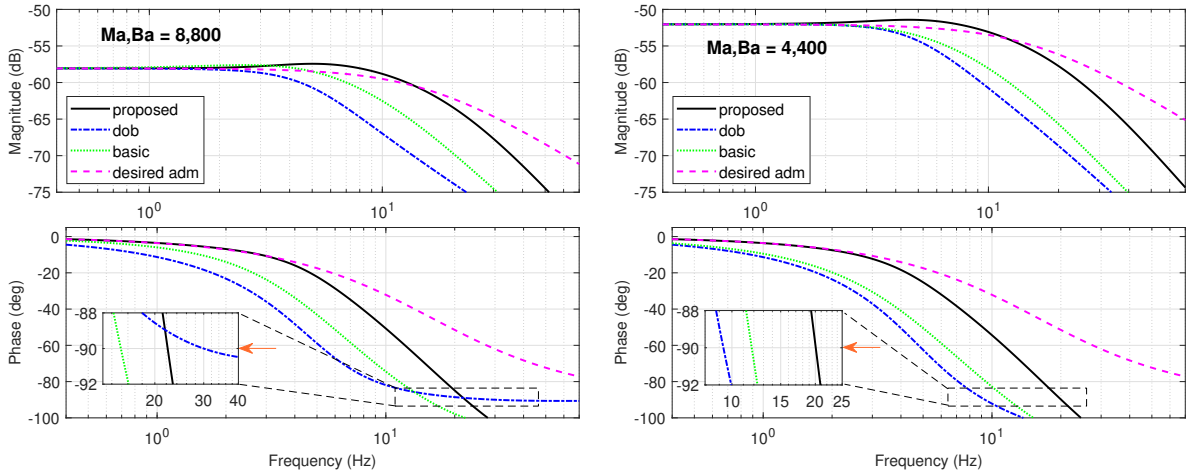

Fig. 3. Magnitude and Phase characteristics of $Y(s)$ to evaluate admittance rendering and contact stability performances of all the methods at large and small values of M_a and B_a. The proposed method exhibits improved desired admittance tracking and enhanced contact stability.

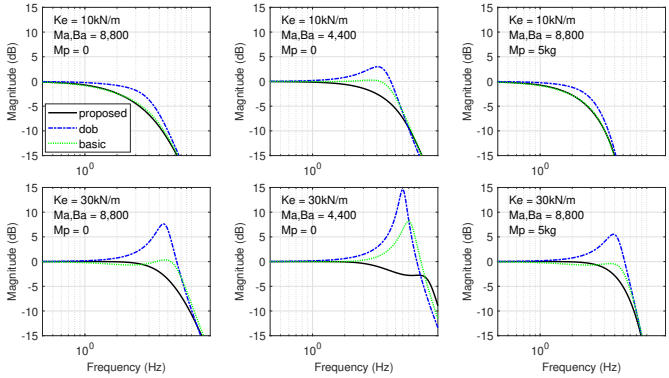

Fig. 4. Magnitude characteristics of $H(s)$ when $Q = 1$ to evaluate contact resonances at soft (K_e = 10kN/m) and hard (K_e = 30kN/m) contacts with varying values of M_a,B_a and the effect of adding extra payload to the end effector.

IV. Experimental Verification

In this section, the proposed method is implemented and co-manipulation in Fig. 1(b) and autonomous operation Fig. 1(c) tasks are executed to validate the theoretical analyses conducted in the previous section.

A. Controller and Robot Parameter Determination

The controller and robot dynamics parameters are experimentally determined by a nonparametric system identification technique. Under position control, a Schroeder multisine, which is utilized as an excitation signal, is supplied as the desired position in Z-axis motion and the position response of the robot in Z-direction is measured by the encoders. These measurements and the command signal are differentiated using a LPF with high cutoff frequency to obtain velocities from which an empirical transfer function is calculated. The model $T = CR/(1 + CR)$ is then fit to obtain the values utilized in theoretical analyses as shown in (8) and (9). Parameters utilized for controller implementation in experiments are empirically tuned from (9) as $T_n(s) = (100s + 400)/(2.5s^2 + 120s + 400)$ and $\omega_Q = 15$ Hz, unless specified. The admittance controller values utilized in Fig. 3 are utilized in the experiments to match experimental results to the theoretical ones.

B. Controller Implementation

Since the COMAU RACER robot software platform accepts position commands, the transfer functions in Fig. 2 are translated to produce position commands as

$$\mathcal{X}_i = \frac{A}{s(1-Q)}\mathcal{F}_r - \frac{A(1+QC_n^{-1}R_n^{-1})}{s(1-Q)}\mathcal{F}_m - \frac{QT_n^{-1}}{s(1-Q)}\mathcal{V}_m. \quad (20)$$

For faster implementation and tuning between test cycles, the transfer functions in (20) are discretized with a Tustin transformation in MATLAB at a sample time of 0.0008 s and the result is sent to the robot external controller using the `rosparam` command of the ROS package in MATLAB, where they are executed in real-time.

C. Experimental Validation of Contact Stability and Reduced Peak Contact Forces

Contact control experiments are conducted in autonomous mode to validate the analysis in Section III. Three cases of contact on soft and hard surfaces without payload and contact on soft surface with added payload (extra 5 Kg) are considered as illustrated in Fig. 1(c). The contact surface is a 3D printed plastic beam cantilevered into the robot's workspace. Here, it is desired that the peak force on first contact, settling time, and the steady-state error be reduced. Under admittance control, the robot is commanded to start from the same position by applying a virtual constant force, $F_r = 16$ N, which forces the robot to move and makes contact with the plastic beam. The results for all the three cases are presented in Figs. 5, 6, & 7, respectively for various admittance controller values. Moreover, numerical values of peak contact forces and RMS errors at steady-state

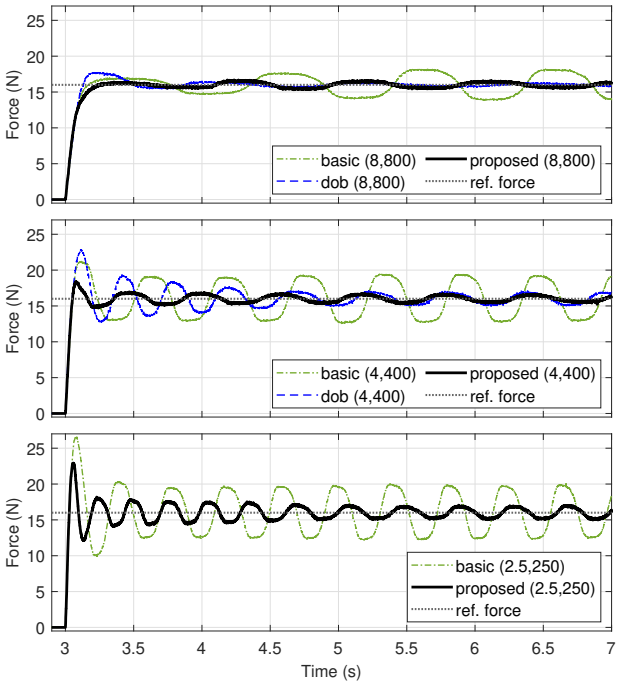

Fig. 5. Contact control on soft surfaces.

TABLE I

PEAK CONTACT FORCE AND RMSE VALUES FOR FIGS. 5 & 6

	Soft surface		Hard surface	
METHOD at (Ma,Ba) setting	Peak force at contact (N)	RMSE at steady-state (N)	Peak force at contact (N)	RMSE at steady-state (N)
basic (8,800)	17.02	1.67	30.87	13.49
dob (8,800)	17.78	0.18	-	-
proposed (8,800)	16.41	0.33	27.11	4.34
basic (4,400)	21.23	2.62	51.59	16.07
dob (4,400)	22.99	0.69	48.11	2.41
proposed (4,400)	18.38	0.39	28.12	0.28
basic (2.5,250)	26.59	2.90	-	-
proposed (2.5,250)	22.92	0.65	-	-

are presented in Table I for no payload case and Table II for extra payload case.

In all the results, the proposed method exhibits the lowest values of peak contact forces and steady-state errors. Moreover, it shows the fastest settling time even when $M_a, B_a = 2.5, 250$, an indication of suppressing the effects of high-frequency contact forces to enhance contact stability. On the other hand, the dob shows better performance when $M_a, B_a = 8,800$ but exhibits large oscillations at steady-state when $M_a, B_a = 4,400$. The same scenario is observed for the basic method.

To conclude, the above experimental results agree with the increased frequency at which the passivity condition is violated for the proposed method in Fig. 3 and reduced peak contact forces even with added payload in Fig. 4. Poor performance shown by large peak contact forces and oscillations at steady-state also validate the theory for the basic and dob methods in Figs. 3 & 4.

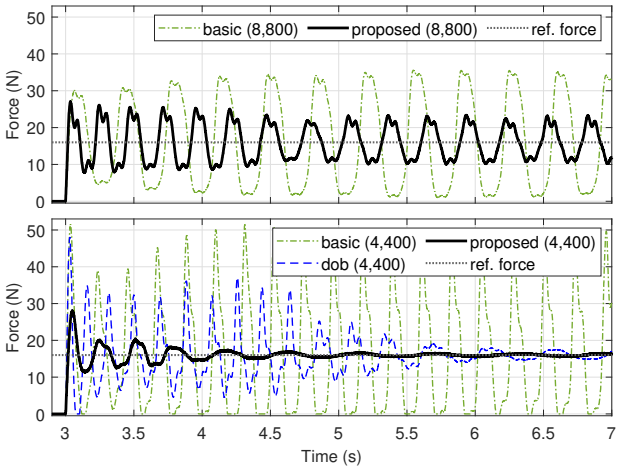

Fig. 6. Contact control on hard surfaces.

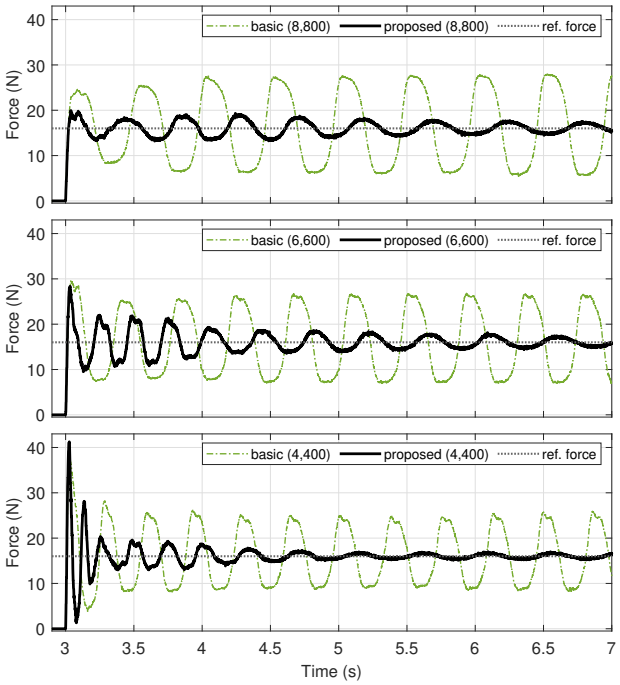

Fig. 7. Soft surface: effect of adding payload.

TABLE II

PEAK CONTACT FORCE AND RMSE VALUES FOR FIG. 7

METHOD at (Ma,Ba) setting	Peak force at contact (N)	RMSE at steady-state (N)
basic (8,800)	24.64	8.74
proposed (8,800)	19.93	1.07
basic (6,600)	29.60	7.64
proposed (6,600)	28.37	1.12
basic (4,400)	39.78	6.23
proposed (4,400)	41.25	0.44

D. Actual Demonstrations of Complex Assembly Tasks with Manual Guidance of the Robot

The switch insertion task in Fig. 1(b) and more two tasks of plug insertion with fine positioning and colliding the gripper tip with random objects are conducted. The plug and switch insertion tasks are conducted with only linear motion of the robot activated, i.e., with only joints 1/2/3, while the the third experiment of contacting random objects is conducted with all the joints including rotation of the end-effector activated, i.e., joints 1-6. In all these tasks, the human manipulates the admittance controlled robot as illustrated in Fig. 1(b). The video attached to this paper, also accessible via `https://youtu.be/8XfkdHEdWDs`, shows the demos along with the live plots of x/y/z force responses. As compared to the basic method, the proposed method is observed to exhibit smallest contact forces, faster damping, and no oscillations during contact. Moreover, the proposed method maintains stability even when the switch is stuck in the rail.

V. Conclusion

The experimental results agree with the theoretical analyses that with the proposed method, the admittance can be expanded in terms of gain and cutoff frequency without bandwidth limitation from the inner loop dynamics while maintaining contact stability. Extended works involved incorporating payload compensation feature in the design of the proposed method. The extended method is called Combined Dynamics Observer (CDYOB) in [23]. Moreover, a comparative study of the proposed method with the Outer-Loop Integrated DOB in task space (OIDOBt) in [24] and the Multi-Function Observer (MOB) in [25] is also conducted in [23] since these methods are related. In addition, we plan to implement all the three methods to various multi-DOF systems other than industrial manipulators.

References

[1] M. R. Pedersen, L. Nalpantidis, R. S. Andersen, C. Schou, S. Bøgh, V. Krüger, and O. Madsen, "Robot skills for manufacturing: From concept to industrial deployment," *Robotics and Computer-Integrated Manufacturing*, vol. 37, pp. 282–291, 2016.

[2] A. Umbrico, A. Cesta, and A. Orlandini, "Enhancing awareness of industrial robots in collaborative manufacturing," *Semantic Web*, no. Preprint, pp. 1–40.

[3] H. Chen and J. Xiao, "Robust compliant assembly automation using an industrial robot," in *2011 6th IEEE Conference on Industrial Electronics and Applications*, pp. 1161–1166, IEEE, 2011.

[4] T. Tang, H.-C. Lin, Y. Zhao, Y. Fan, W. Chen, and M. Tomizuka, "Teach industrial robots peg-hole-insertion by human demonstration," in *2016 IEEE International Conference on Advanced Intelligent Mechatronics (AIM)*, pp. 488–494, IEEE, 2016.

[5] W. Chung, C. Rhee, Y. Shim, H. Lee, and S. Park, "Door-opening control of a service robot using the multifingered robot hand," *IEEE Transactions on Industrial Electronics*, vol. 56, no. 10, pp. 3975–3984, 2009.

[6] J. Li, J. Tao, L. Ding, H. Gao, Z. Deng, and K. Xia, "Twisting door handles and pulling open doors with a mobile manipulator," in *2015 IEEE International Conference on Robotics and Biomimetics (ROBIO)*, pp. 686–691, IEEE, 2015.

[7] M. Stuede, K. Nuelle, S. Tappe, and T. Ortmaier, "Door opening and traversal with an industrial cartesian impedance controlled mobile robot," in *2019 International Conference on Robotics and Automation (ICRA)*, pp. 966–972, IEEE, 2019.

[8] J. Arents and M. Greitans, "Smart industrial robot control trends, challenges and opportunities within manufacturing," *Applied Sciences*, vol. 12, no. 2, p. 937, 2022.

[9] A. Q. Keemink, H. van der Kooij, and A. H. Stienen, "Admittance control for physical human–robot interaction," *The International Journal of Robotics Research*, vol. 37, pp. 1421–1444, Sept. 2018.

[10] X. Yu, P. Liu, W. He, Y. Liu, Q. Chen, and L. Ding, "Human-robot variable impedance skills transfer learning based on dynamic movement primitives," *IEEE Robotics and Automation Letters*, vol. 7, no. 3, pp. 6463–6470, 2022.

[11] D. Ko, D. Lee, W. K. Chung, and K. Kim, "On the performance and passivity of admittance control with feed-forward input," in *2022 IEEE/RSJ International Conference on Intelligent Robots and Systems (IROS)*, pp. 11209–11215, IEEE, 2022.

[12] S. Haddadin, A. De Luca, and A. Albu-Schäffer, "Robot collisions: A survey on detection, isolation, and identification," *IEEE Transactions on Robotics*, vol. 33, no. 6, pp. 1292–1312, 2017.

[13] K. Haninger and D. Surdilovic, "Bounded collision force by the sobolev norm: compliance and control for interactive robots," in *2019 IEEE international conference on robotics and automation (ICRA)*, pp. 8259–8535, 2019.

[14] A. Sidiropoulos, F. Dimeas, D. Papageorgiou, T. Prapavesis Semetzidis, Z. Doulgeri, A. Zanella, F. Grella, K. Sagar, M. Jilich, A. Albini, G. Cannata, and M. Zoppi, "Safe and Effective Collaboration With a High-Payload Robot: A Framework Integrating Novel Hardware and Software Modules," *IEEE Robotics & Automation Magazine*, pp. 2–11, 2024.

[15] K. Samuel, *Development of Advanced Robot Force Control Algorithms*. PhD thesis, DGIST, 2023.

[16] K. Haninger, M. Radke, A. Vick, and J. Kruger, "Towards High-Payload Admittance Control for Manual Guidance with Environmental Contact," *IEEE Robotics and Automation Letters*, 2022.

[17] D. Surdilovic, "Robust control design of impedance control for industrial robots," in *2007 IEEE/RSJ International Conference on Intelligent Robots and Systems*, pp. 3572–3579, IEEE, 2007.

[18] H. Pham and Q.-C. Pham, "Convex Controller Synthesis for Robot Contact," *IEEE Robot. Autom. Lett.*, vol. 5, pp. 3330–3337, Apr. 2020.

[19] K. Ohnishi, M. Shibata, and T. Murakami, "Motion control for advanced mechatronics," *Mechatronics, IEEE/ASME Transactions on*, vol. 1, no. 1, pp. 56–67, 1996.

[20] E. Sariyildiz and K. Ohnishi, "On the explicit robust force control via disturbance observer," *Industrial Electronics, IEEE Transactions on*, vol. 62, no. 3, pp. 1581–1589, 2015.

[21] K. Samuel, K. Haninger, and S. Oh, "High-performance admittance control of an industrial robot via disturbance observer," in *IECON 2022–48th Annual Conference of the IEEE Industrial Electronics Society*, pp. 1–6, IEEE, 2022.

[22] K. Samuel, K. Haninger, and S. Oh, "Increasing admittance of industrial robots by velocity feedback inner-loop shaping," in *2023 IEEE International Conference on Robotics and Automation (ICRA)*, pp. 5228–5234, IEEE, 2023.

[23] K. Samuel, K. Haninger, R. Oboe, S. Haddadin, and S. Oh, "A perturbation-robust framework for admittance control of robotic systems with high-stiffness contacts and heavy payload," *IEEE Robotics and Automation Letters*, vol. 9, no. 7, pp. 6432–6439, 2024.

[24] K. Samuel, K. Haninger, R. Oboe, and S. Oh, "Task space outer-loop integrated dob-based admittance control of an industrial robot," *IEEE Transactions on Control Systems Technology*, vol. 32, no. 3, pp. 974–989, 2024.

[25] K. Samuel, K. Haninger, R. Oboe, and S. Oh, "Outer-loop admittance and motion control dual improvement via a multi-function observer," *IEEE Transactions on Industrial Electronics*, vol. 71, no. 8, pp. 9339–9350, 2024.